Equivalent Strut Model for Seismic Design of Steel Moment Connections Reinforced with Ribs

리브로 보강된 철골 모멘트 접합부의 내진설계를 위한 등가 스트럿 모델

이 철 호*
Lee, Cheol Ho

국문요약

본 논문에서는 리브로 보강된 철골 모멘트 접합부의 내진설계법 정립을 위한 등가 스트럿 모델을 제시하였다. 리브 보강 접합부의 응력전달 메커니즘은 고전 휨이론에 의한 예측과는 전혀 다르며, 리브는 리브의 기울기 방향으로 스트럿 거동을 보임을 유한요소해석에 의해 밝혔다. 리브를 스트럿 요소로 파악하여 리브 접합부의 실용설계에 활용될 수 있는 등가 스트럿 모델링 방안을 제시하였다.

주요어 : 철골모멘트접합부, 내진설계, 리브, 스트럿 거동

ABSTRACT

This paper presents an equivalent strut model for seismic design of steel moment connections reinforced with ribs. It is shown from the finite element analysis results that the force transfer mechanism in the rib connections is completely different from that predicted by the classical beam theory and a clear strut action in the ribs does exist. By treating the rib as a strut, an equivalent strut model that could be used as the basis of a practical design procedure is proposed.

Key words : steel moment connection, seismic design, rib, strut action

1. Introduction

The 1994 Northridge earthquake in California caused widespread brittle fracture in connections of steel moment-resisting frames. A variety of improved moment connection details were proposed after the earthquake. Two key strategies to circumvent the problems associated with the pre-Northridge connection include strengthening the connection or weakening the beams that frame into the connection.[1] The aim is to shift the plastic hinging away from the face of the column, thus reducing the possibility of brittle failure conditions. Fig. 1 shows one such connection details per strengthening strategy.[2]

The rib connections have been demonstrated to perform well in the full-scale test conducted by Zekioglu et al..[2] In this case, rib reinforcement was used to supplement the taper-cut reduced beam section(RBS), i.e., to further limit the stress in the beam flange welds and to provide increased redundancy for the connection. Rib reinforcement may also be used to address the situation where the frame design requires an excessive RBS(greater than 50% of the beam flange) due to short spans, or larger beam depths. However, a design procedure for the rib connection has not been established yet. Engineers often use rib plates to enhance the seismic performance of welded steel moment connections, thinking that the moment of inertia is increased near the face of the column so that the tensile stress in the groove weld is reduced. Previous studies have indicated that the classical beam theory cannot provide reliable force transfer predictions in the steel moment connections with welded haunch.[3]-[6] Especially, it was shown in Lee-Uang's studies[4],[5] that an inclined strip in the web of the straight haunch acts as a strut rather than following the beam theory. Lee-Uang viewed the web of straight haunch as a vertical rib plate and the haunch flange as a stability element. It was speculated that there exists close link between the rib and the straight haunch.

In this study, employing the beam theory for the design of rib-reinforced steel moment connections is brought into question first. An equivalent strut model that could be used as the basis of a design procedure is then proposed.

2. Numerical simulation and internal stress distributions

To gain insight into the behavior of the rib connection,

* 정회원 · 경남대학교 건축학부, 교수(대표저자 : chlee@kyungnam.ac.kr)
본 논문에 대한 토의를 2001년 8월 31일까지 학회로 보내 주시면 그 결과를 게재하겠습니다. (논문접수일 : 2001. 4. 19 / 심사종료일 : 2001. 5. 10)

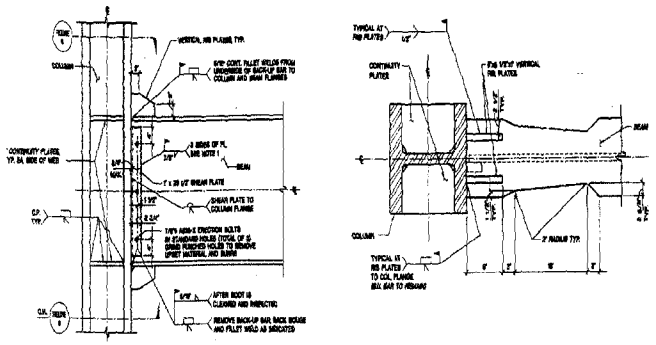

Fig. 1 Rib-reinforced connection(specimen COH1)[2]

the test specimen COH-1 from the full-scale tests conducted by Zekioglu et al.[2] was modeled and analyzed using the general-purpose finite element analysis program ABAQUS.[7] Fig. 2 shows the test setup. The specimen consisted of W27×178 beam(W706×792) and W14×455 column(W483×2025). The test specimen COH-1 had a rib length of 229mm (9 in), a rib height of 165mm(6.5 in), and a rib thickness of 25mm(1 in). Both the flanges and web of the beam and column were modeled with the 8-node continuum element (element type C3D8 in ABAQUS). The beam web was directly connected to the column flange in the model. Fig. 3 shows the finite element mesh in the connection region.

Steel material properties obtained from tensile coupon tests were used. Material nonlinearity with the von Mises yielding criterion was considered in the analysis. The analytically predicted load versus beam tip deflection relationship was correlated with the response envelope of the test result in Fig. 4. The correlation was reasonable. The finite element model was then used to investigate the stress distribution in the connection region.

Plastic hinging of the beam is often assumed to occur at the rib tip. However it is difficult to justify this assumption due to "light" reinforcement nature of the rib. Some positive

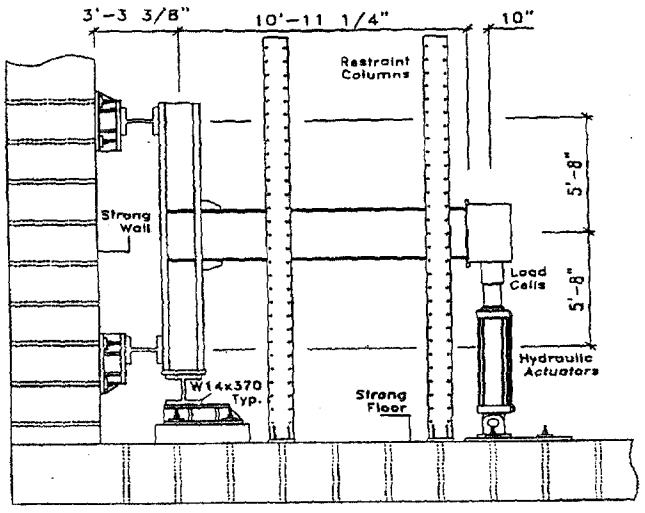

Fig 2 Test setup for the specimen COH-1

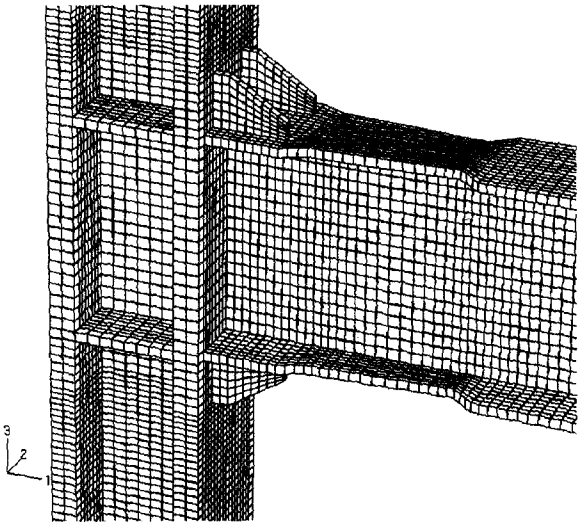

Fig. 3 Finite element mesh for the specimen COH-1

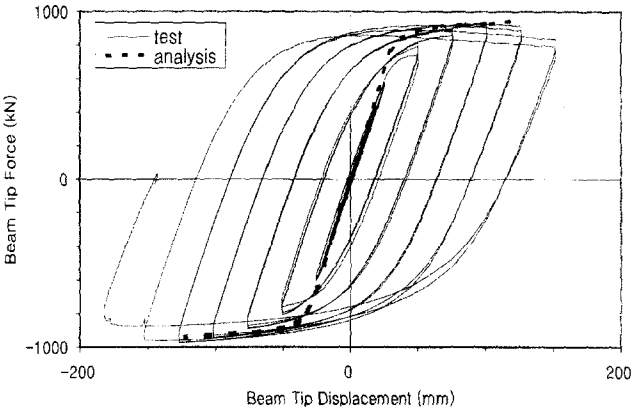

Fig. 4 Correlation of analytical and experimental global responses

measures such as the RBS are desirable to maintain the rib region truly elastic by pushing the plastic hinging of the beam away from the rib region.

Typical rib connection assumed in this study is shown in Fig. 5, where the radius-cut RBS is introduced to effectively confine the plastic hinging of the beam outside the rib region. Since the rib region is expected to remain essentially elastic under this scheme, an elastic analysis with a 712KN (160kips) load applied at the beam tip was conducted to study the force transfer mechanism of the connection.

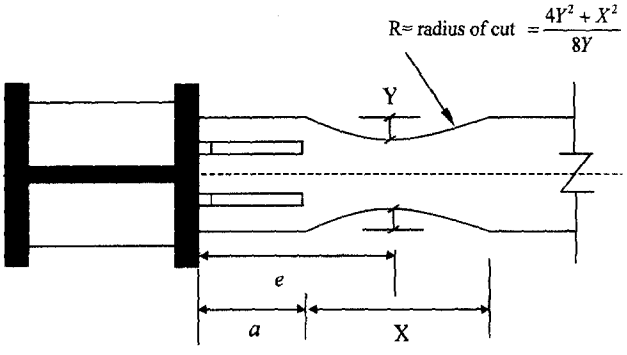

Fig. 5 Rib connection supplemented by radius-cut RBS

Based on the analysis results, the flexural stress profile at the column face is presented in Fig. 6. The flexural stress profile from the beam theory by treating the beam and ribs as an integral section is also presented. It is evident from this figure that the force transfer mechanism in the rib connection cannot be reliably predicted by the beam theory. Note that the beam theory underestimates significantly the stress at the beam flanges, i.e., the stress in the beam flange groove welds.

Fig. 7 shows the percentage of the beam shear transferred by each element at the face of the column. The ribs transfer 168% of the beam shear applied and produces reverse shear in the beam web. Again this phenomenon cannot be explained by the beam theory. The principal stress distribution in the rib in Fig. 8 suggests clear diagonal strut action in the rib. This strut action of the rib can be used to explain the reverse shear phenomenon noted above.

Analyses were performed to investigate the stress distribution at the beam-rib interface. In addition to analyzing the test specimen COH-1 with a rib length, a, of 229mm(9 in), a rib height, b, of 165mm(6.5 in), and a rib thickness, t, of 25mm (in), additional cases were also included in the parametric study by varying the rib slope and the rib thickness within some practical ranges. Similar parametric study was also conducted for the single rib configuration(see Fig. 9(a)).

The normal and shear stress distributions along the beam-rib interface are presented in Fig. 10, where the stress profile of each case has been normalized by the maximum stress and the distance has been normalized by the rib length. Similar distributions were also obtained when the rib thickness was varied(results not shown). Fig. 10(a) shows that the resultant normal force, N, is located approximately at a distance of 0.60a from the face of the column. Fig. 10(b) shows that the shear stress profile is insensitive to the variation of rib length. The total shear force at the beam-rib interface is defined as Q. The resultant from force components N and Q, and the associated angle are listed in Table 1. As was suggested from the principal stress plot in Fig. 8, the resultant angle of Q and N reasonably matches the rib diagonal angle.

Fig. 11 compares the deformed shapes of the single and dual rib configurations. It is noted that the load path of the single rib configuration is more direct because all of the beam web, rib and column web plates exist in the co-plane and it does not accompany the beam flange bending which is unavoidable in the dual rib configuration(see Fig. 11(b)).

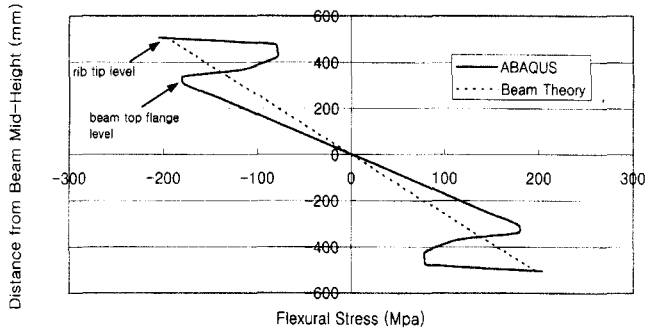

Fig. 6 Comparison of flexural stress profiles along beam depth (specimen COH-1)

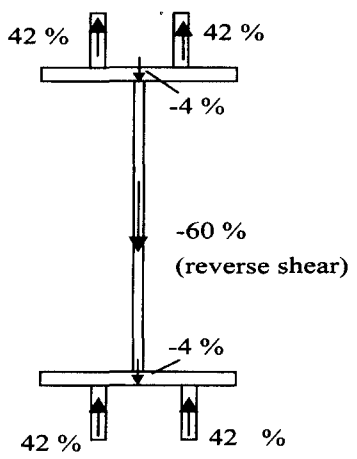

Fig. 7 Shear transfer at the column face

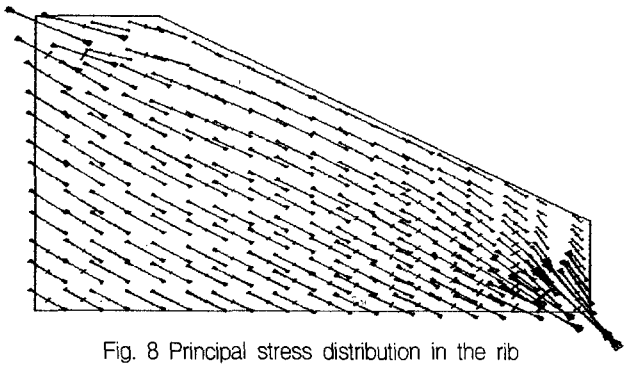

Fig. 8 Principal stress distribution in the rib

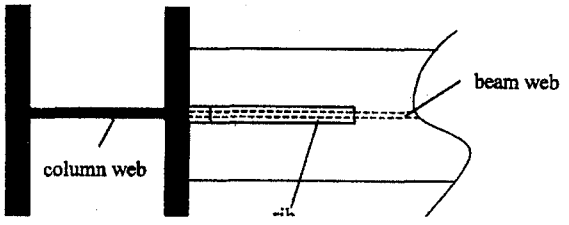

(a) single rib type

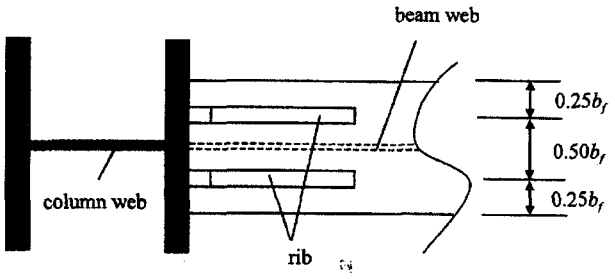

(b) dual rib type

Fig. 9 Two types of rib configuration

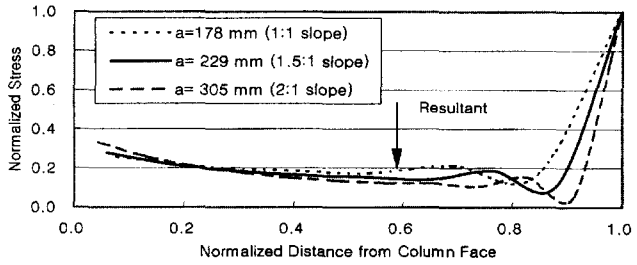

(a) Normal stress distribution

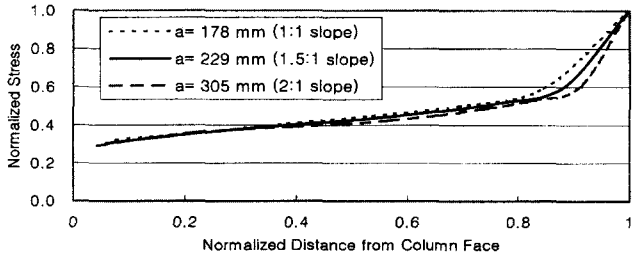

(b) Shear stress distribution

Fig. 10 Typical normal and shear stress distributions along beam-rib

Table 1 Comparison of rib diagonal and resultant angles

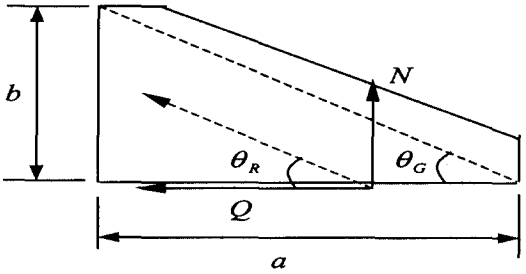

$\theta_G = \tan^{-1}(b/a)$ (degree)	$\theta_R = \tan^{-1}(N/Q)$ (degree)	
	Single rib type	Dual rib type
42.9	39.4	41.8
35.8	35.2	36.1
28.4	30.9	32.9

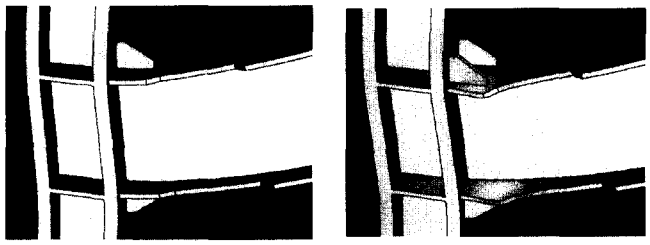

(a) Single rib type (b) Dual rib type

Fig. 11 Comparison of deformed shapes

Accordingly it is expected that the load transferred by one rib in the dual rib configuration will be smaller than that by one rib in the single rib configuration under the same rib thickness. To confirm this expectation, Q and N values from the finite element analysis for both configurations are compared in Table 2.

Table 2 Comparison of Q and N values in single and dual rib configurations

	Single rib		Dual rib	
	Q	N	Q^*	N^*
a=178mm (1:1 slope)	1.0	1.0	0.99**	0.98
a=229mm (1.5:1 slope)	1.0	1.0	1.09	1.10
a=305mm (2:1 slope)	1.0	1.0	1.15	1.15

* sum of two ribs
** relative values

It is observed from this table that the load transfer of the single rib configuration is about two times that of one rib in the dual rib configuration. Additional analyses also confirmed this observation. This information is important in designing the connection with the dual rib configuration. All these observations were incorporated in developing an equivalent strut model in the following section.

3. Equivalent strut model

Based on the observations from the finite element analysis in the previous section, an equivalent strut model which considers the strut action in the rib is proposed for practical design purposes. First, the equivalent strut area, A_e, is defined as, (Fig. 12)

$$A_e = \frac{\eta(ab - c^2)t}{\sqrt{(a-c)^2 + (b-c)^2}} \quad (1)$$

where A_e= equivalent strut area, a= rib length, b= rib height, c= cut length, t= rib tickness, and η = equivalent strut area factor.

The proposed equivalent strut model is presented in Fig. 13, where V_{pd} is the design beam shear force which corresponds to the strain-hardened plastic hinging at the narrowest section in the RBS(see Fig. 5). Following the

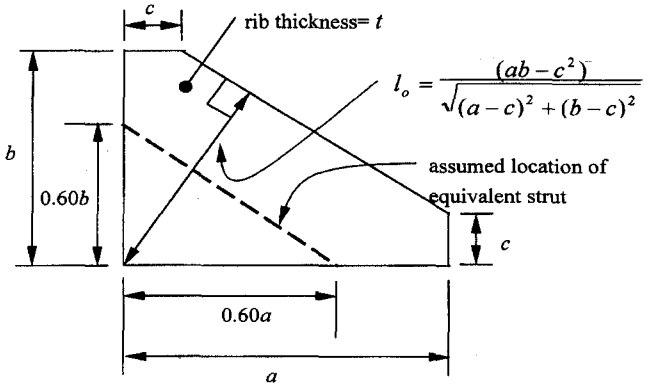

Fig. 12 Definition of rib cross section width

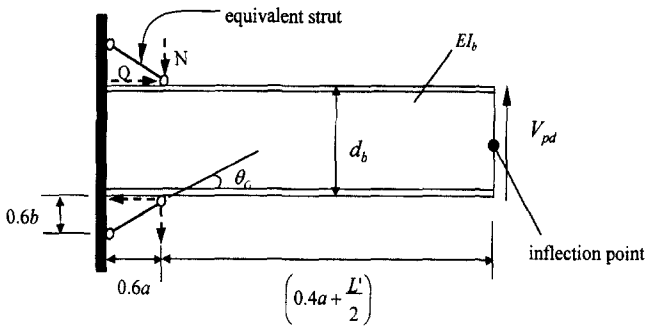

Fig. 13 Equivalent strut model

AISC Seismic Provisions[8], the beam plastic moment is

$$M_{pd}=1.1Z_{RBS}F_{ye} \tag{2}$$

where Z_{RBS} and F_{ye} are the plastic section modulus at the narrowest section in the RBS and expected yield strength of the beam, respectively. The corresponding beam shear is then

$$V_{pd}=\frac{M_{pd}}{\left(\frac{L'}{2}+a-e\right)}+V_G \tag{3}$$

where V_G is the beam shear due to gravity load between beam plastic hinges, and L' is the beam span length between rib tips. See Fig. 5 for the definition of e. In the model, rib is replaced by an equivalent strut(i.e., a simple truss element). The angle and location of the strut incorporate the findings from the finite element analysis results. The equivalent strut force corresponds to the resultant of Q and N at the beam-rib interface in the actual connection. The remaining problem is to determine the equivalent area factor, η, in a way which will give the strut force present in the actual rib. Theoretically the number of degrees of freedom along the beam-rib interface is infinite. It is hardly feasible to determine the equivalent area factor by purely analytical method due to both the continum problem nature and the complexity of the boundary conditions around the rib connection. Semi-analytical approach is adopted in this study. Fig. 14 shows the interaction model for deformation compatibility of the proposed equivalent strut model.

The normal force, N, can be computed with reasonable accuracy by using Eq. (4).

$$N=\left(\frac{b}{a}\right)Q \tag{4}$$

Then the horizontal shear force, Q, remains as the only unknown. This unknown can be determined by applying horizontal deformation compatibility condition at the strut tip(point A in Fig. 14).

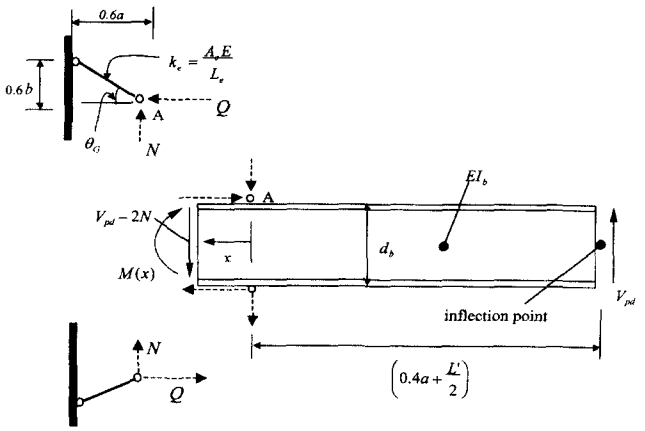

Fig. 14 Interaction model for deformation compatibility of equivalent strut model

Horizontal displacement component of equivalent strut at point A : d_x(strut)

By referring to Fig. 12 and Fig. 14, axial stiffness of the equivalent strut, k_e, is computed as Eq. (5).

$$k_e=\frac{A_eE}{L_e}=\frac{\eta(ab-c^2)tE}{(0.60)\sqrt{(a^2+b^2)}\sqrt{(a-c)^2+(b-c)^2}} \tag{5}$$

where $L_e=(0.60)\sqrt{(a^2+b^2)}$ (6)

E=Young's modulus

The horizontal displacement component of the equivalent strut at point A is thus obtained by dividing Q with k_e as follows.

$$d_x(strut)=\frac{\sqrt{Q^2+N^2}\cos(\theta_G)}{k_e}=\frac{Q}{k_e}$$
$$=\frac{(0.60)\sqrt{(a^2+b^2)}\sqrt{(a-c)^2+(b-c)^2}}{\eta(ab-c^2)tE}\times Q \tag{7}$$

Horizontal displacement component of beam flange at point A : d_x(beam)

From Fig. 14, the beam moment within the equivalent strut region is

$$M(x)=V_{pd}(x+0.40a+L'/2)-2Nx-Qd_b$$
$$=V_{pd}(x+0.40a+L'/2)-2\left(\frac{b}{a}\right)Qx-Qd_b \tag{8}$$

Note that Eq. (4) was inserted into Eq. (8). The beam moment produces a compressive strain in the beam top flange.

$$\varepsilon(x)_{flange}=\frac{M(x)}{EI_b}\times\frac{d_b}{2} \tag{9}$$

The horizontal component of the beam deformation at point A is thus obtained by integrating the axial strain of the beam top flange within the equivalent strut region as follows.

$$d_x(beam) = \int_0^{0.60a} \varepsilon(x)_{flange}\, dx = \frac{d_b}{2EI_b}\int_0^{0.60a} M(x)dx$$
$$= \frac{(0.21a^2+0.15aL')d_b}{EI_b} \times V_{pd}$$
$$-\left(\frac{0.18abd_b+0.30ad_b^2}{EI_b}\right)\times Q \qquad (10)$$

The unknown force, Q, can be solved by equating Eq. (7) and Eq. (10) for deformation compatibility :

$$Q = \frac{\left(\frac{(0.21a+0.15L')ad_b}{I_b}\right)}{\left(\frac{1}{\eta}\right)\frac{(0.60)\sqrt{(a^2+b^2)}\sqrt{(a-c)^2+(b-c^2)}}{(ab-c^2)t}+\frac{(0.18b+0.30d_b)(ad_b)}{I_b}} \times V_{pd} \qquad (11)$$

To calibrate the equivalent strut area factor for practical design purposes, the horizontal shear force values, Q, obtained from the finite element analysis within some practical range of the rib slope and thickness were inserted into Eq. (11). The results are summarized in Table 3. Although the factors vary more or less depending on the rib slope and thickness, they are fairly stable. The average value is close to 1.50. With an equivalent area factor of 1.50, Table 4 shows the degree of accuracy of Q and N values predicted by using Eqs. (4) and (11). Using larger equivalent area factor (say, 1.80) produces only slightly conservative predictions.

Table 3 Equivalent strut area factors

	Rib thickness		
	0.6t (=15mm)	1.0t (=25mm)	1.4t (=35mm)
a=178mm (1:1 slope)	1.65	1.44	1.31
a=229mm (1.5:1 slope)	1.72	1.52	1.31
a=305mm (2:1 slope)	1.85	1.65	1.48

Table 4 Predictions of Q and N values with η=1.50

	Q			N		
	Rib thickness			Rib thickness		
	0.6t (=15mm)	1.0t (=25mm)	1.4t (=35mm)	0.6t (=15mm)	1.0t (=25mm)	1.4t (=35mm)
a=178mm (1:1 slope)	0.93*	1.03	1.09	0.99	0.96	1.01
a=229mm (1.5:1 slope)	0.91	0.99	1.08	0.91	1.02	1.11
a=305mm (2:1 slope)	0.86	0.94	1.01	0.76	1.14	0.92

* predicted values were normalized by the corresponding finite element analysis results

Thus it is recommended, for practical design purposes, that the equivalent area factor, η, be taken as

$$\eta = 1.50 \qquad (12)$$

4. Prediction of beam flange groove weld stress

Knowing the two interface forces, the moment at the column face is

$$M_f = V_{pd}(a+L'/2) - Qd_b - 2N(0.60a) \qquad (13)$$

The flexural stress, f_{bf}, in the beam flange groove can be calculated by the elementary mechanics as follows.

$$f_{bf} = \frac{M_f}{I_b}\left(\frac{d_b}{2}\right) = \frac{V_{pd}(a+L'/2) - Qd_b - 1.2Na}{S} \qquad (14)$$

where S is the elastic section modulus of the beam. The flexural stresses based on Eq. (14) are compared in Fig. 15 with the flexural stress profiles obtained from both the classical beam theory and the finite element analysis. The flexural stress obtained from Eq. (14) is very satisfactory.

Based on the equivalent strut model described above, a step-by-step design procedure for the rib connection has been also recommended(Lee, et al., 2001).[9] Detailed presentation is omitted here due to space limitation.

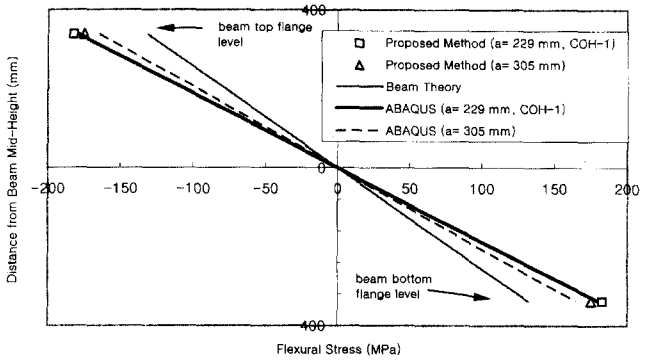

Fig. 15 Comparison of beam flange groove weld flexural stress predictions

5. Conclusions

Main conclusions on the equivalent strut model for the seismic design of steel moment connections reinforced with ribs are summarized as follows.

(1) The rib drastically changes the force transfer mechanism that cannot be predicted reliably by the classical beam theory. The flexural stress prediction from the beam theory by treating the beam and ribs as an integral section significantly underestimates the stress in the

beam flange groove welds. Diagonal strip in the rib acts as a strut and this strut action tends to produce reverse shear in the beam web.

(2) Both high shear and normal stresses exist at the interface between the beam and rib. Idealizing the rib as a strut, an equivalent strut model was proposed that could be used to determine the interaction forces at the interface between the beam and rib. With an equivalent strut area factor of 1.50, the proposed method provided satisfactory predictions. The results of this study are directly usable in developing a rational seismic design procedure of rib-reinforced steel moment connections.

Acknowledgments

Financial support provided by the Korea Earthquake Engineering Research Center(KEERC) under Grant No. 2000G0206 is gratefully acknowledged.

References

1. Bruneau, M., Uang, C. M., and Whittaker, A., *Ductile Design of Steel Structures*, MaGraw-Hill, New York, NY., 1998.
2. Zekioglu, A., Mozaffarian, H., Chang, K. L., and Uang, C. M., "Designing After Northridge," *Modern Steel Construction*, Vol. 37, No. 3, 1997, pp. 36-42.
3. Lee, C. H. and Uang, C. M., "Analytical modeling of dual panel zone in haunch repaired steel MRFs," *J. Struct. Engrg.*, ASCE, Vol. 123, No. 1, 1997, pp. 20-29.
4. Lee, C. H. and Uang, C. M., "Analytical modeling of seismic steel moment connections with welded straight haunch," *Proc. of SEEBUS 2000*, Kyoto, Japan, 2000. 10. 21-22, pp. 131-140
5. Lee, C. H. and Uang, C. M., "Analytical modeling and seismic design of steel moment connections with welded straight haunch," (accepted by *J. Struct. Engrg.*, ASCE, in-press)
6. Yu, Q. S., Uang, C. M., and Gross, J., "Seismic rehabilitation design of steel moment connection with welded haunch," *J. Struct. Engrg*, ASCE, Vol. 126, No. 1, 2000, pp. 69-78.
7. HKS, *ABAQUS Users Manual, Version 5.8*, Hibbit, Karlson & Sorenson, Inc., 1998
8. AISC, *Seismic Provisions for Structural Steel Buildings*, 2nd Ed., AISC, Chicago, IL, 1997.
9. Lee, C. H., Lee, J. K., and Kwon, K. T., "Analytical modeling and design method for rib-reinforced seismic steel moment connections," *2000 KEERC Report*, 2001, pp. 135-157.